

## ANOMALOUS BEHAVIORS OF ELASTIC MODULI, DC CONDUCTIVITY AND OPTICAL PROPERTIES IN MIXED TRANSITION–METAL–ION (20-*x*) MnO<sub>2</sub>–*x*Fe<sub>2</sub>O<sub>3</sub>–80TeO<sub>2</sub> TELLURITE GLASS SYSTEM

R. HISAM, A. K. YAHYA\*

*School of Physics and Materials Studies, Universiti Teknologi Mara, 40450 Shah Alam, Selangor, Malaysia*

Mixed transition–metal–ion  $x\text{Fe}_2\text{O}_3$ –(20- $x$ )MnO<sub>2</sub>–80TeO<sub>2</sub> glasses were prepared using melt-quenching method to study the DC conductivity, elastic and optical properties of the glasses. DC conductivity showed a strong increase for  $x \leq 10$  mol% Fe<sub>2</sub>O<sub>3</sub> before reaching a saddle-like behavior between 10 mol %  $\leq x \leq 15$  mol%, followed by a large increase for  $x > 15$  mol%. Longitudinal and shear velocities  $v_L$  and  $v_S$  exhibited non-linear behaviors and where both increased for  $x \leq 10$  mol% with an anomalous drop at  $x = 15$  mol% Fe<sub>2</sub>O<sub>3</sub>, followed by a large increase at  $x > 15$  mol%. Independent longitudinal modulus ( $C_L$ ), shear modulus ( $\mu$ ) and bulk modulus ( $K_c$ ) showed similar behaviors to both velocities. Hardness ( $H$ ), Debye temperature ( $\theta_D$ ) and glass transition temperature ( $T_g$ ) also substantially increased for  $x \leq 10$  mol% before reaching a saddle-like behavior between 10 and 15 mol% Fe<sub>2</sub>O<sub>3</sub>. Subsequently, a slight increase at  $x > 15$  mol% was observed. The anomalous region between 10 mol%  $\leq x \leq 15$  mol% coincided with DC conductivity saddle-like region and is suggested to be related to the mixed transition–ion effect (MTE). Meanwhile, in same region, optical band gap ( $E_{opt}$ ) exhibited a maxima, whereas refractive index showed a minima, thereby indicating a variation in polarizability due to the changes in concentration of bridging and non-bridging oxygens.

(Received February 4, 2016; Accepted April 11, 2016)

*Keywords:* Elastic moduli; Tellurite glass; Ultrasonic velocity; Optical energy gap; Mixed transition-ion effect

### 1. Introduction

Oxide glasses have been extensively studied because of their unique properties and potential applications in many industries. Interestingly, among the oxide glasses, tellurium oxide-based glasses have drawn technical interest because of their low melting point [1–7] and high glass forming ability [8–10]. Tellurium oxide-based glasses are non-hygroscopic, unlike phosphate and borate glasses [11]. These glasses possess a high refractive index [12–17], significant third-order nonlinear optical susceptibility [18–20], low maximum phonon energy [21], and high dielectric constant [22–24], which make these glasses a potential material for optical devices. In addition, tellurite glasses are stable against devitrification, non-toxic, and resistant to moisture for long periods [25]. The basic structure of the glass is characterized by a TeO<sub>4</sub> trigonal bipyramid (tbp) and TeO<sub>3</sub> trigonal pyramid (tp) unit structure with a lone pair at the equatorial position [26]. Interestingly, TeO<sub>2</sub> is a recognized conditional glass former, which requires the addition of a modifier oxide, such as alkali, alkaline earth, and transition metal oxides or other glass formers [27–28].

The addition of transition–metal–ions (TMI) with more than one valence state, such as V<sub>2</sub>O<sub>5</sub>, CuO<sub>2</sub>, NiO, and Fe<sub>2</sub>O<sub>3</sub>, resulted in oxide glasses exhibiting semiconducting properties [29–34], wherein conduction can occur by electron transfer from ions in the lower valence state to those in a higher valence state [33,35]. Interestingly, several glasses containing two TMI showed non-linear variation in certain properties such as resistivity, AC conductivity, and dielectric

---

\* Corresponding author: ahmad191@salam.uitm.edu.my

properties [36, 37]. The non-linear variation in these properties is called the mixed transition-ion-effect (MTE). MTE was reported in several glasses including tellurite,  $\text{Fe}_2\text{O}_3\text{-MnO}_2\text{-TeO}_2$  [38],  $\text{Fe}_2\text{O}_3\text{-MnO-TeO}_2$  [35],  $\text{Fe}_2\text{O}_3\text{-BaO-V}_2\text{O}_5$  [36], and  $\text{Fe}_2\text{O}_3\text{-V}_2\text{O}_5\text{-P}_2\text{O}_5$  [37]. For these mixed-TMI systems, conductivity minimum attributed to MTE was observed. For the  $x\text{V}_2\text{O}_5\text{-(50-x)}\text{Fe}_2\text{O}_3\text{-50P}_2\text{O}_5$  glass system, the conductivity minimum at  $x = 20$  mol% was attributed to enhance localization caused by increased configurational disorder when two transition ions were mixed in a glass system, thereby hindering electronic motion and reducing conductivity [37]. MTE was also reported for the  $x\text{Fe}_2\text{O}_3\text{-(20-x)}\text{MnO-80TeO}_2$  glass system where DC resistivity and activation energy maximum were observed at  $x = 8.5$  mol% [35]. The position of these conductivity minima were below the TMI ratio of 0.5 where these minima are highly expected. According to Dutta et al., localization that occurs in glasses involves electron bandwidth ( $B$ ) and the magnitude of random potential ( $V_0$ ) where localization is expected to occur at maximum  $V_0/B$  ratio, thereby translating to a TMI ratio of roughly 0.5. Interestingly, AC conductivity properties of a mixed TMI  $x\text{Fe}_2\text{O}_3\text{-(20-x)}\text{MnO}_2\text{-80TeO}_2$  glass system were minimized at  $x = 15$  mol%, which was higher than the TMI ratio of 0.5 [38]. However, dielectric studies of the same glass system showed a minimum at  $x = 10$  mol% [38]. The dielectric minima was attributed to some form of blocking effect on heavy dipoles because of MTE. The presence of two different minima for AC conductivity and dielectric constant is intriguing and indicates that MTE behavior needs to be investigated further. This phenomenon also presents the possibility that varying contributions between two different ions may exist because two different minimum values were observed in the glass system.

Although several studies on mixed TMI glass systems are available [35–37], these works were mostly conductivity studies, although some works included optical investigation. However, other properties such as dielectric, optical and elastic properties are also expected to be influenced by MTE. Studies on these properties will provide a better understanding of the MTE mechanism in mixed-TMI glasses. Interestingly, elastic studies on mixed-TMI glass systems, such as  $\text{MoO}_3\text{-V}_2\text{O}_5\text{-TeO}_2$  [9],  $\text{NiO-V}_2\text{O}_5\text{-TeO}_2$  [39], and  $\text{MnO}_2\text{-V}_2\text{O}_5\text{-P}_2\text{O}_5$  [40] glasses, have exhibited non-linear behavior in bulk modulus ( $K_c$ ), Young's Modulus ( $E$ ), and shear modulus ( $\mu$ ). However, no specific investigation addresses the non-linear region where conductivity minimum caused by MTE was observed. Studying the elastic properties of mixed-TMI glasses in the conductivity anomaly region is important because this will provide insight on the elastic nature of MTE. Meanwhile, the result of a number of studies on the elastic properties of mixed electronic-ionic glass systems, such as  $35\text{V}_2\text{O}_5\text{-(65-x)}\text{TeO}_2\text{-xLi}_2\text{O}$  glass system [41], have exhibited a significant reduction in ultrasonic velocity and independent elastic moduli in the region of electronic-to-ionic transition, indicating that the electronic-ionic transition involves changes in elastic properties. However, such observation was not reported for mixed-TMI glasses.

Aside from elastic properties, investigating the optical properties in the MTE region is also crucial. Interestingly, analysis of the optical properties in mixed-TMI  $(60-x)\text{V}_2\text{O}_5\text{-40TeO}_2\text{-xMoO}_3$  glass revealed an anomalous slope change at  $x = 40$  mol% [9]. However, it is not clear if the anomaly is related to MTE because conductivity anomaly was not reported. Nevertheless, a recent observation of a maxima in optical absorption in the MTE region of  $\text{Fe}_2\text{O}_3\text{-MnO-TeO}$  systems provides motivation for a more detailed study [35]. Furthermore, optical gap  $E_g$  and refractive index  $n$  of the  $\text{Fe}_2\text{O}_3\text{-MnO}_2\text{-TeO}$  glass system in the MTE region were not reported.

In the present work, we investigated the elastic and optical properties in the conductivity minimum region of  $x\text{Fe}_2\text{O}_3\text{-(20-x)}\text{MnO}_2\text{-80TeO}_2$  glasses. To verify the elastic nature of the MTE, glass transition  $T_g$  of the system was also measured to correlate the results with the rigidity changes of the glass. In addition, quantitative analysis using bulk compression [11, 42] and ring deformation [11] models was carried out to obtain additional information on glass network behavior in the region under compression.

## 2. Experimental details

### 2.1 Glass preparation

Ternary  $80\text{TeO}_2\text{-xFe}_2\text{O}_3\text{-(20-x)}\text{MnO}_2$  glasses with  $x = 2$  mol% to 20 mol% were prepared by adopting a melt-quenching method by initially mixing appropriate amounts of high purity

(>99.95%) powders of  $\text{TeO}_2$ ,  $\text{Fe}_2\text{O}_3$ , and  $\text{MnO}_2$ . The mixture was homogenized using an agate mortar, placed in a ceramic crucible, and heated in a box furnace at 1273 K for 1 h. The melted mixture was quickly poured into a stainless steel mold and kept at room temperature. The sample was polished using fine sand paper to a thickness of approximately 3.5–6.5 mm to produce parallel opposite surfaces for ultrasonic velocity measurements.

## 2.2 Glass characterization

Density ( $\rho$ ) of the glass samples was determined using Archimedes method, which utilized toluene as an immersion medium at room temperature. Molar volume ( $V_a$ ) was obtained according to the following equation [43]:

$$V_a = M_{\text{glass}}/\rho_{\text{glass}} \quad (1)$$

where  $M_{\text{glass}}$  and  $\rho_{\text{glass}}$  are the molar mass and the density of the glass, respectively. The amorphous nature of these glass samples was established and confirmed using X-ray diffraction (XRD). Ultrasonic velocity measurements were carried out at 5 MHz in both shear and longitudinal modes by employing the pulse–echo technique at room temperature using RITEC RAM-500-M6 high performance ultrasonic system. The elastic moduli and related quantities were calculated using the following equations [41].

$$\text{Longitudinal modulus, } C_L = v_L^2 \rho \quad (2)$$

$$\text{Shear modulus, } \mu = v_s^2 \rho \quad (3)$$

$$\text{Bulk modulus, } K_e = C_L - \frac{4}{3}\mu \quad (4)$$

$$\text{Young's modulus, } E = \frac{9K\mu}{3K + \mu} \quad (5)$$

$$\text{Debye temperature, } \theta_D = \left(\frac{h}{k_b}\right) \left(\frac{3PN_A}{4\pi V_a}\right)^{\frac{1}{3}} v_m \quad (6)$$

$$\text{Poisson's ratio, } \sigma = \frac{C_L - 2\mu}{2(C_L - \mu)} \quad (7)$$

$$\text{Hardness, } H = \frac{(1 - 2\sigma)E}{6(1 + \sigma)} \quad (8)$$

$$\text{Mean sound velocity, } v_m = \left[\frac{3v_L^3 v_s^3}{v_L^3 + 2v_s^3}\right]^{\frac{1}{3}} \quad (9)$$

where  $h$  is Planck's constant,  $k_b$  is Boltzmann's constant,  $N_A$  is Avogadro's number,  $V_a$  is the molar atomic volume, and  $P$  is the number of atoms in the chemical formula.

The optical absorption spectra of the glass powder samples were recorded using a double-beam Shimadzu UV-VIS-NIR spectrophotometer model in the wavelength range of 200–1000 nm at room temperature.  $T_g$  of all glass samples was obtained using a differential scanning calorimeter (NETZSCH, DSC 200 F3) at a heating rate of 10 °C min<sup>-1</sup>. The DC conductivity of the glass samples were measured using a High-Resolution Dielectric Analyzer (Novocontrol) connected with a BDS 1200 sample holder over a frequency range of 10<sup>-2</sup> Hz to 10<sup>6</sup> Hz with an applied potential of 1 V and temperature range of 303 K to 473 K.

### 3. Results and analysis

The variation of density ( $\rho$ ) and molar volume ( $V_a$ ) with  $\text{Fe}_2\text{O}_3$  content for the  $x\text{Fe}_2\text{O}_3-(20-x)\text{MnO}_2-80\text{TeO}_2$  ( $x = 2-20$  mol%) glass system is presented in Fig. 1. The figure indicates that density decreased from  $5175 \text{ kg}\cdot\text{m}^{-3}$  ( $x = 2$  mol%) to  $4915 \text{ kg}\cdot\text{m}^{-3}$  ( $x = 20$  mol%), whereas molar volume increased from  $x = 2$  mol% to  $x = 20$  mol%. The decrease in density ( $\rho$ ) may be attributed to the increase in molar volume ( $V_a$ ) (Table 1). The differences in molecular volume between  $\text{MnO}_2$  with lower molecular volume of ( $17.28 \text{ cm}^3\text{mol}^{-1}$ ) and  $\text{Fe}_2\text{O}_3$  with higher molecular volume ( $30.48 \text{ cm}^3\text{mol}^{-1}$ ) could be the reason for the increase in molar volume ( $V_a$ ). However, our detailed analysis indicated that the unexpected existence of different regions in  $V_a$  may be related to MTE. The variation of  $V_a$  (Fig. 1) can be divided into three regions, which started with a relatively high increase rate (4.27%) between  $x = 2$  mol% and  $x = 5$  mol%, followed by a slower increase rate (2.52%) between  $x = 10$  mol% and  $x = 15$  mol% and a final increase at a rate of 1.82% between  $x = 18$  mol% and  $x = 20$  mol%. Meanwhile, density ( $\rho$ ) decreased from  $5175 \text{ kg}\cdot\text{m}^{-3}$  ( $x = 2$  mol%) to  $5038 \text{ kg}\cdot\text{m}^{-3}$  ( $x = 5$  mol%) before achieving a saddle-like behavior between 10 and 15 mol%  $\text{Fe}_2\text{O}_3$  followed by a slight decrease ( $x > 15$  mol%). The saddle-like behavior in 10 mol%  $\leq x \leq 15$  mol% coincided with the MTE for the same glass system, as previously reported. The amorphous nature of the  $x\text{Fe}_2\text{O}_3-(20-x)\text{MnO}_2-80\text{TeO}_2$  ( $x = 2-20$  mol%) glass samples was confirmed, as previously reported [38]. The effect of  $\text{Fe}_2\text{O}_3$  on the structure of the glasses was investigated using FTIR, which was also reported in the literature [38]. Meanwhile, DC conductivity (Fig.2) generally increased with increasing  $\text{Fe}_2\text{O}_3$  content except for  $x = 15$  mol%. The DC conductivity between  $x = 10$  mol% and 15 mol% points formed a flat region which coincides with the density saddle-like region as shown in Figure 1.

Table 1. Values of density ( $\rho$ ), molar volume ( $V_a$ ), longitudinal velocity ( $v_L$ ), shear velocity ( $v_s$ ) and mean velocity ( $v_m$ ) of  $(20-x)\text{MnO}_2-x\text{Fe}_2\text{O}_3-80\text{TeO}_2$  glass system.

$x$ (mol.%)	$\rho$ ( $\text{kg}\cdot\text{m}^{-3}$ ) $\pm 3$	$V_a$ ( $\text{m}^3\cdot\text{mol}^{-1}$ ) $\times 10^{-5}$ $\pm 0.001$	$v_L$ ( $\text{km}\cdot\text{s}^{-1}$ ) $\pm 0.01$	$v_s$ ( $\text{km}\cdot\text{s}^{-1}$ ) $\pm 0.01$	$v_m$ ( $\text{km}\cdot\text{s}^{-1}$ ) $\pm 0.01$
2	5175	2.831	3.38	1.92	2.10
5	5038	2.952	3.43	1.95	2.20
10	4977	3.061	3.59	2.06	2.30
15	4971	3.138	3.54	2.04	2.30
18	4958	3.190	3.69	2.14	2.40
20	4915	3.248	3.71	2.15	2.40

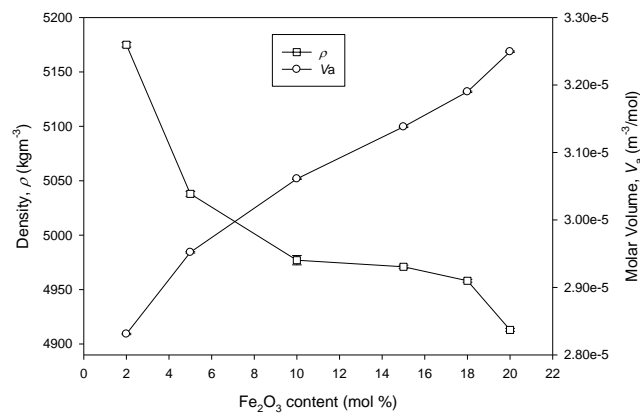


Fig.1. Molar volume ( $V_a$ ) and density ( $\rho$ ) of the  $(20-x)\text{MnO}_2-x\text{Fe}_2\text{O}_3-80\text{TeO}_2$  ( $x = 2$  mol% to 20 mol%) glass samples.

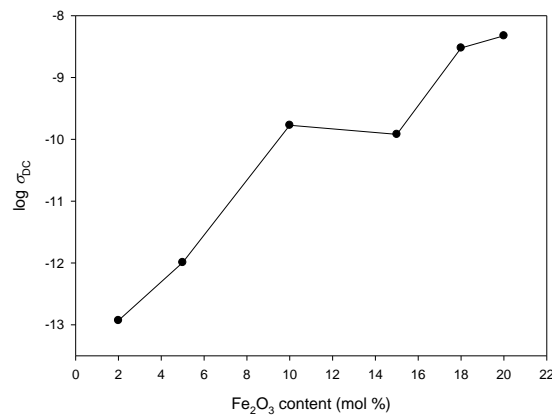


Fig.2. Variation of DC conductivity with  $Fe_2O_3$  content  $(20-x)MnO_2-xFe_2O_3-80TeO_2$  ( $x = 2$  mol% to 20 mol%) glass samples at room temperature.

Generally, velocity for both modes increased with  $Fe_2O_3$  content except for a slight decrease at  $x=15$  mol% (Fig. 3).  $C_L$ ,  $\mu$ ,  $K_e$ , and  $E$  gradually increased between 2 mol%  $\leq x \leq 5$  mol% and 18 mol%  $\leq x \leq 20$  mol% (Figs. 4 and 5). Between the two regions, the moduli increased, except at  $x=15$  mol% where softening behavior was observed. Poisson's ratio ( $\sigma$ ) (Fig. 6) decreased with  $Fe_2O_3$  for 2 mol%  $\leq x \leq 10$  mol%, but was relatively unchanged between 10 and 20 mol% (10 mol%  $\leq x \leq 20$  mol%). However, hardness  $H$  (Fig. 6) increased, except for 10 mol%  $\leq x \leq 15$  mol%, which coincided with the density of the saddle-like region.  $\theta_D$  and  $v_m$  (Fig.7) increased with  $Fe_2O_3$  except for 10 mol%  $\leq x \leq 15$  mol% in which a slight change in  $\theta_D$  and  $v_m$  was observed. Meanwhile, glass transition temperature  $T_g$  of the glass system increased from 343.3 °C ( $x = 2$  mol%) to 423.5 °C ( $x = 20$  mol%) after adding  $Fe_2O_3$  (Table 2). However, in the 10 mol%  $\leq x \leq 15$  mol% region,  $T_g$  was almost unchanged with a percentage change of only of 0.2%.

Table 2. Values of longitudinal modulus ( $C_L$ ), shear modulus ( $\mu$ ), bulk modulus ( $K_e$ ), Young's modulus ( $E$ ), hardness ( $H$ ), Poisson's ratio ( $\sigma$ ), Debye temperature ( $\theta_D$ ) and glass transition temperature ( $T_g$ ) of  $(20-x)MnO_2-xFe_2O_3-80TeO_2$  glass system.

$x$ (mol.%)	$C_L$ (GPa) $\pm 0.3$	$\mu$ (GPa) $\pm$ 0.2	$K_e$ (GPa) $\pm$ 0.5	$E$ (GPa) $\pm 2.0$	$H$ (GPa) $\pm 0.2$	$\theta_D$ (K) $\pm$ 0.4	$\sigma$ $\pm 0.01$	$T_g$ (°C) $\pm 2$	$\Delta T_g$
2	59.2	19.1	33.7	48.3	3.0	222.0	0.26	343.3	-
5	59.3	19.2	33.7	48.4	3.1	229.0	0.26	359.7	16.4
10	64.0	21.1	35.9	52.9	3.5	245.0	0.25	388.8	29.1
15	62.4	20.8	34.7	52.0	3.5	246.0	0.25	389.0	0.2
18	67.7	22.6	37.5	56.5	3.8	259.0	0.25	420.3	31.3
20	67.8	22.8	37.5	56.8	3.8	260.0	0.25	423.5	3

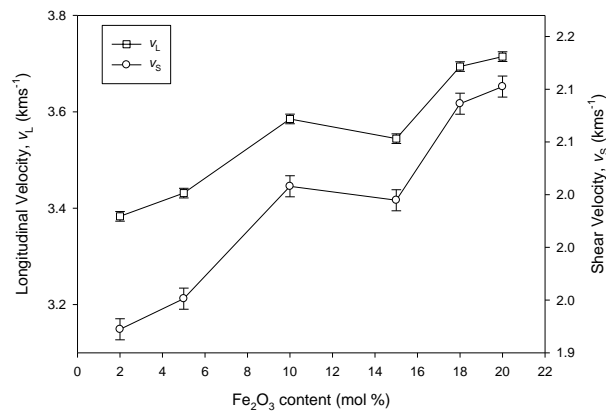


Fig.3. Longitudinal velocity ( $v_L$ ) and shear velocity ( $v_s$ ) versus  $Fe_2O_3$  content of the  $(20-x)MnO_2-xFe_2O_3-80TeO_2$  ( $x = 2$  mol% to 20 mol%) glass samples.

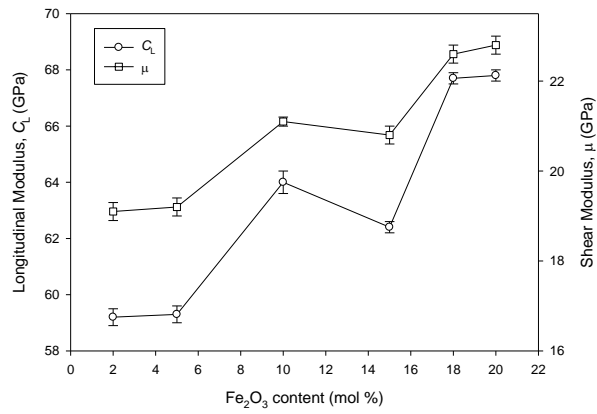


Fig.4. Plot of longitudinal modulus ( $C_L$ ), shear modulus ( $\mu$ ), with  $Fe_2O_3$  content of  $(20-x)MnO_2-xFe_2O_3-80TeO_2$  ( $x = 2$  mol% to 20 mol%) glass samples.

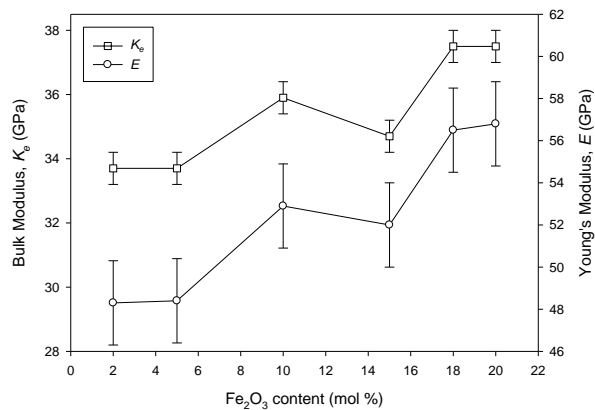


Fig.5. Bulk modulus ( $K_b$ ) and Young's modulus ( $E$ ) versus  $Fe_2O_3$  content of the  $(20-x)MnO_2-xFe_2O_3-80TeO_2$  ( $x = 2$  mol% to 20 mol%) glass samples

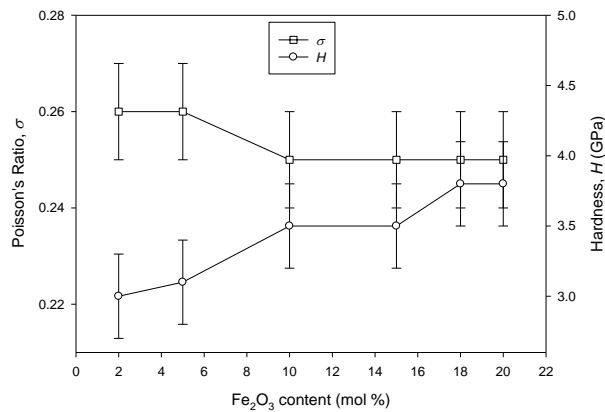


Fig.6. Poisson's ratio ( $\sigma$ ) and Hardness ( $H$ ) versus  $Fe_2O_3$  content of the  $(20-x)MnO_2-xFe_2O_3-80TeO_2$  ( $x = 2$  mol% to 20 mol%) glass samples.

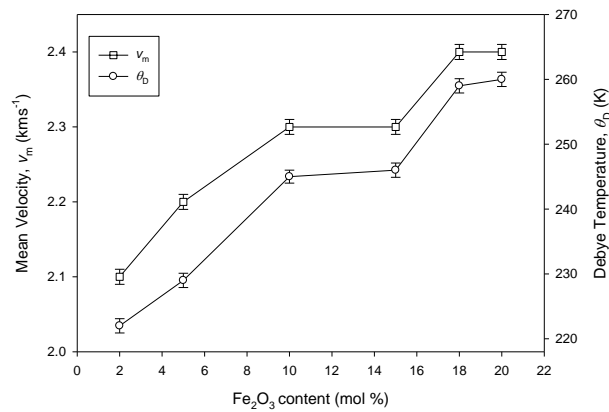


Fig.7. Mean velocity ( $v_m$ ) and Debye temperature ( $\theta_D$ ) versus  $Fe_2O_3$  content of the  $(20-x)MnO_2-xFe_2O_3-80TeO_2$  ( $x = 2$  mol% to 20 mol%) glass samples

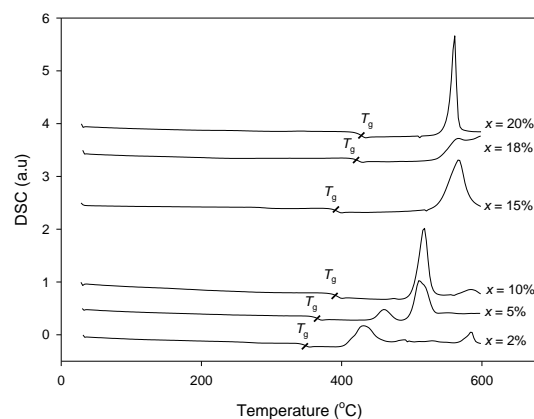


Fig. 8. DSC curves of the  $(20-x)MnO_2-xFe_2O_3-80TeO_2$  ( $x = 2$  mol% to 20 mol%) glass.

The elastic properties of the glass system were further analyzed using a bulk compression model in concurrence with a ring deformation model. In the bulk compression model, the compression of the glass network is assumed to be isotropic and changes bond lengths without changing bond angles [11]. Based on the bulk compression model, the ideal bulk modulus of an oxide glass can be expressed in the following equations [11,42]:

$$K_{bc} = n_b r^2 F / 9 \quad (10)$$

where  $r$  is the bond length ( $r$  of  $\text{TeO}_2 = 0.199$  nm,  $r$  of  $\text{Fe}_2\text{O}_3 = 0.195$  nm, and  $r$  of  $\text{MnO}_2 = 0.189$  nm [46]) and  $F$  is the stretching force constant ( $F$  of  $\text{TeO}_2 = 216$  N.m<sup>-1</sup>,  $F$  of  $\text{Fe}_2\text{O}_3 = 229$  N.m<sup>-1</sup>, and  $F$  of  $\text{MnO}_2 = 251$  N.m<sup>-1</sup> [46]) [11,42]:

$$F = 1.7/r^3 \quad (11)$$

$n_b$  is the number of network bonds per unit volume [11,42]:

$$n_b = n_f N_A / V_a \quad (12)$$

where  $n_f$  is the number network bonds per unit glass formula ( $n_f$  of  $\text{TeO}_2 = 4$ ,  $n_f$  of  $\text{Fe}_2\text{O}_3 = 6$ , and  $n_f$  of  $\text{MnO}_2 = 4$  [46]),  $N_A$  is Avogadro's number, and  $V_a$  is the molar volume.

For polycomponent oxide glasses with  $i$  different types of network bonds [11], Eq. (10) can be written as follows [11,46]:

$$K_{bc} = N_A / 9 V_a \sum_i (x n_f F r^2)_i \quad (13)$$

where  $x$  is the mole fraction of oxide glass and  $F$  is the stretching force constant (Table 3).

Table 3. Values of cation–anion bond length ( $r$ ), stretching force constant ( $F$ ) and coordination number ( $n_f$ ) of the oxides of  $\text{TeO}_2$ ,  $\text{MnO}_2$  and  $\text{Fe}_2\text{O}_3$ .

Oxide	$r$ (nm)	$F$ (Nm <sup>-1</sup> )	$n_f$	References
$\text{TeO}_2$	0.1990	216	4	[11,46]
$\text{MnO}_2$	0.1891	251	4	[11,46]
$\text{Fe}_2\text{O}_3$	0.1945	231	6	[11,46]

Table 4 shows the variation of bulk modulus ( $K_{bc}$ ), ratio of  $K_{bc}/K_e$ , number of bond per unit volume ( $n_b$ ), average force constant ( $\bar{F}$ ) and average crosslink density ( $\bar{n}_c$ ). In the bulk compression model, we assumed that an isotropic deformation model resulted in changes in network bond length ( $l$ ) and sizes without changing bond angles. In this model, bond compression depended on the bond stretching force constant. Based on this model, an isotropic ring compression mechanism was observed when  $K_{bc}/K_e = 1$ . By contrast, other mechanisms, such as ring deformation, may exist when  $K_{bc}/K_e > 1$ . On one hand, variation in  $K_{bc}$  gradually decreased from 82.45 GPa to 78.96 GPa (at  $x = 2$  mol% to  $x = 15$  mol%) before slightly increasing to 81.75 GPa ( $x = 18$  mol%). Beyond  $x > 18$  mol%,  $K_{bc}$  decreased to 76.77 GPa ( $x = 20$  mol%). On the other hand, the  $K_{bc}/K_e$  ratio decreased with  $\text{Fe}_2\text{O}_3$  addition of up to 10 mol% before slightly increasing at  $x = 15$  mol%. For  $x > 18$  mol%,  $K_{bc}/K_e$  ratio decreased from 2.18 ( $x = 18$  mol%) to 2.08 ( $x = 20$  mol%).

Table 4. The values of theoretical bulk modulus ( $K_{bc}$ ), ratio of ( $K_{bc}/K_e$ ), number of network bond per unit volume ( $n_b$ ), average ring size ( $\ell$ ), average stretching force constant ( $\bar{F}$ ) average cross-link density ( $\bar{n}_c$ ) of (20-x)MnO<sub>2</sub>-xFe<sub>2</sub>O<sub>3</sub>-80TeO<sub>2</sub> glass system.

x(mol%)	$K_{bc}$ (GPa) $\pm$ 0.03	$K_{bc}/K_e$ $\pm$ 0.03	$n_b \times 10^{28}$ (m <sup>-1</sup> ) $\pm$ 0.01	$\ell$ (nm) $\pm$ 0.008	$\bar{F}$ (N.m <sup>-1</sup> )	$\bar{n}_c$
2	82.45	2.45	8.60	0.508	234	2.1
5	80.25	2.38	8.36	0.507	232	2.2
10	79.15	2.20	8.26	0.497	230	2.4
15	78.96	2.28	8.25	0.500	229	2.5
18	81.75	2.18	8.23	0.491	228	2.6
20	76.77	2.08	8.25	0.490	227	2.7

Based on the bulk compression model [47], the average crosslink density of the glass network ( $\bar{n}_c$ ) is expressed as follows [11, 42]:

$$\bar{n}_c = \frac{1}{\eta} \sum_i (n_c)(N_c) \quad (14)$$

where  $n_c$  is the number of crosslinks per cation,  $N_c$  is the number of cation per glass formula unit, and  $\eta$  is the total number of cations per glass formula unit. The average ideal crosslink density of the oxide glass increased from 2.1 to 2.7 with the addition of Fe<sub>2</sub>O<sub>3</sub> (Table 4). Based on the ring deformation model, depression was not ideally isotropic because some parts of the ring may be deformed because of bending while under compression. Average ring size ( $\ell$ ) is expressed in the following equation [11]:

$$\ell = \left[ 0.0106 \frac{\bar{F}}{K_e} \right]^{0.26} \quad (15)$$

where average stretching force  $\bar{F}$  is expressed as follows [11]:

$$\bar{F} = \frac{\sum (xn_f F)_i}{(xn_f)_i} \quad (16)$$

Variation in  $\ell$  is quite similar to  $K_{bc}/K_e$  (Fig. 9).  $\ell$  (Table 4) decreased gradually from 0.508 nm ( $x = 2$  mol%) to 0.497 nm ( $x = 10$  mol%) before slightly increasing to 0.500 nm ( $x = 15$  mol%).

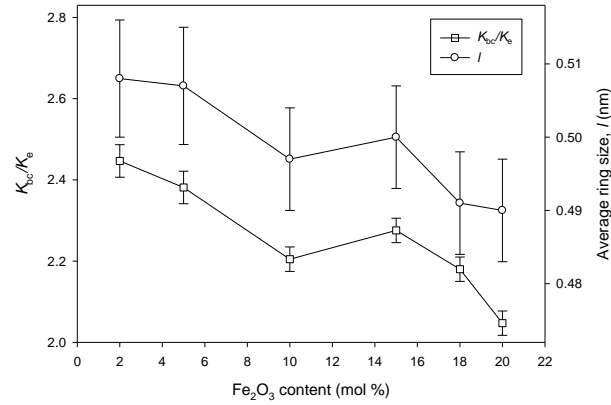


Fig. 9. Plot of  $K_{bc}/K_e$  ratio and average ring size ( $l$ ) with  $Fe_2O_3$  content of the  $(20-x)MnO_2-xFe_2O_3-80TeO_2$  ( $x = 2$  mol.% to 20 mol.%) glass samples.

The optical absorption edge can help clarify optically induced transitions and the optical band gap of materials. Variations in the optical absorption spectrum as a function of the wavelength of the samples did not indicate a sharp absorption edge. Thus, the samples are amorphous. In addition, absorption coefficient  $\alpha$  associated with light that is transmitted out of a sample with thickness  $t$  is obtained using Eq. (17) [11], as follows:

$$I_t = I_0 e^{-\alpha t} \quad (17)$$

where  $I_0$  is the intensity of the incident and  $I_t$  is the intensity of the transmitted radiation. The optical energy gap of the samples was calculated using the empirical relation given by [14], as follows:

$$\alpha(\nu) = B[(h\nu - E_{opt})^2/h\nu] \quad (18)$$

where  $B$  is a constant,  $h\nu$  is the incident photon energy, and  $E_{opt}$  is the optical energy band gap.  $E_{opt}$  was determined by extrapolating the linear region of the plot of  $(\alpha h\nu)^{1/2}$  against  $h\nu$ , where  $(\alpha h\nu)^{1/2} = 0$  (Fig. 10[a-c]). The  $E_{opt}$  values in the range of 1.0 eV to 1.31 eV (Table 5) significantly increased at the initial addition of  $Fe_2O_3$  from 1.07 eV ( $x = 2$  mol%) to 1.31 eV ( $x = 10$  mol%) where maximum  $E_{opt}$  occurs ( $x = 10$  mol%) for the glass system. However,  $E_{opt}$  slightly decreased from 1.31 eV ( $x=10$  mol%) to 1.27 eV at  $x = 15$  mol%, which was followed by a large decrease from 1.27 eV ( $x = 15$ mol%) to  $x = 1.0$  eV ( $x = 20$  mol%).

Table 5. Values of optical band gap ( $E_{opt}$ ), refractive index ( $n$ ), electronic polarizability ( $\alpha_{O_2}$ ) and optical basicity ( $A$ ) of  $(20-x)MnO_2-xFe_2O_3-80TeO_2$  glass system.

$x$ (mol%)	$E_{opt}$ (eV)	$n$	$\alpha_{O_2}^{2-}$	$A$
2	1.07	3.311	3.586	1.204
5	1.09	3.298	3.699	1.219
10	1.31	3.120	3.630	1.210
15	1.27	3.144	3.663	1.214
18	1.09	3.291	3.787	1.229
20	1.0	3.381	3.891	1.241

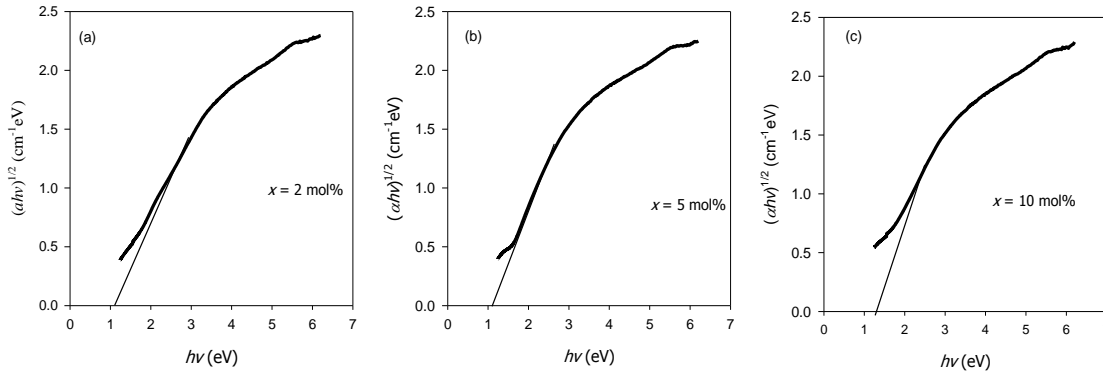


Fig. 10 (a-c)  $(\alpha hv)^{1/2}$  as a function of energy ( $hv$ ) for  $(20-x)\text{MnO}_2-x\text{Fe}_2\text{O}_3-80\text{TeO}_2$  ( $x = 2 \text{ mol\%}$  to  $10 \text{ mol\%}$ ) glass samples.

The values of refractive index  $n$  was obtained from the optical energy gap using the equation [14]:

$$\frac{n^2 - 1}{n^2 + 2} = 1 - \sqrt{\frac{E_{\text{opt}}}{20}} \quad (19)$$

The plot of  $n$  exhibits an opposite behavior compared with  $E_{\text{opt}}$  (Fig. 11) where  $n$  initially decreased from 3.311 ( $x = 2 \text{ mol\%}$ ) to 3.120 ( $x = 10 \text{ mol\%}$ ) followed by slight increase to 3.144 ( $x = 15 \text{ mol\%}$ ) before significantly increasing to 3.381 at  $x = 20 \text{ mol\%}$ . For ternary glasses with a general formula  $X_1\text{A}_p\text{O}_q\text{X}_2\text{B}_r\text{O}_s\text{X}_3\text{C}_n\text{O}_m$  where  $X$  denotes the molar fraction for each oxide, the electronic polarizability of the oxide ion ( $\alpha_{\text{O}_2^-}$ ) is calculated from the optical band gap ( $E_{\text{opt}}$ ) by adopting the following relationship proposed by Dimitrov and Sakka [43];

$$\alpha_{\text{O}_2^-}(E_{\text{opt}}) = [(V_a/2.25)(1 - \sqrt{E_{\text{opt}}/20}) - \sum \alpha_{\text{cat}}]/N_0^{2-} \quad (20)$$

where  $V_a$  is the molar volume,  $\alpha_{\text{cat}}$  is the cation polarizability given by  $X_1p\alpha_A + X_2r\alpha_B + X_3n\alpha_C$  (where molar cation polarizability ( $\alpha$ ) values of  $\text{Fe}^{3+}$ ,  $\text{Mn}^{3+}$ , and  $\text{Te}^{4+}$  ions are  $\alpha_{\text{Fe}}=0.437 \text{ \AA}^3$ ,  $\alpha_{\text{Mn}}=0.437 \text{ \AA}^3$ , and  $\alpha_{\text{Te}}=1.595 \text{ \AA}^3$ , respectively [44]), and  $N_0^{2-}$  is the number of oxide ions in the chemical formula given by  $X_1q + X_2s + X_3m$  [44]. The value of  $\alpha_{\text{O}_2^-}$  (Fig. 12) generally increases with  $\text{Fe}_2\text{O}_3$  except for  $x = 10 \text{ mol\%}$  where a slight decrease in  $\alpha_{\text{O}_2^-}$  was observed. Meanwhile, optical basicity ( $\mathcal{A}$ ) is related to the electron donor power of oxygen in glasses. A significant similarity was observed in the physical background between oxide ion polarizability and optical basicity. The increase of oxide ion polarizability is related to the increase of electron donor power. The relationship between oxide ion polarizability and optical basicity can be expressed in the following equation:

$$\mathcal{A}(E_{\text{opt}}) = 1.67 [(1 - 1/\alpha_{\text{O}_2^-}(E_{\text{opt}}))] \quad (21)$$

The optical basicity values of the glass are calculated and tabulated in Table 5. The value of  $\mathcal{A}$  (Fig. 12) generally increased with  $\text{Fe}_2\text{O}_3$  except for  $x = 10 \text{ mol\%}$ , which showed a slight decrease in  $\mathcal{A}$ .

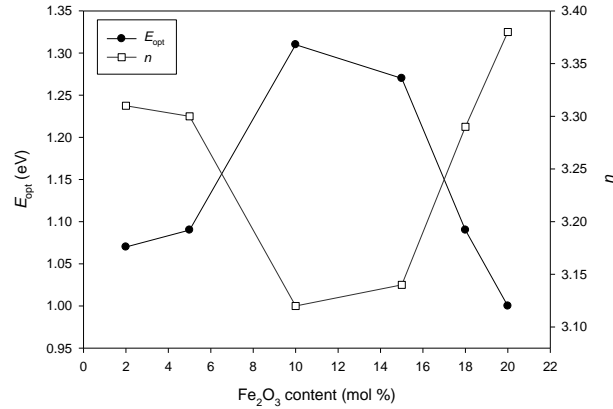


Fig. 11. Plot of  $E_{opt}$  and  $n$  with  $Fe_2O_3$  content  $(20-x)MnO_2-xFe_2O_3-80TeO_2$  ( $x = 2$  mol% to 20 mol%) glass samples.

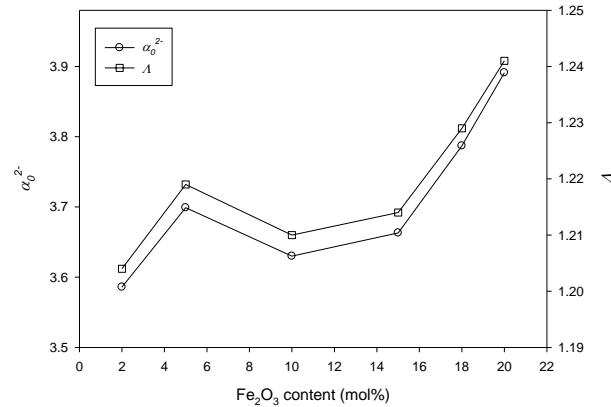


Fig. 12. Plot of  $\alpha_0^{2-}$  and  $A$  with  $Fe_2O_3$  content  $(20-x)MnO_2-xFe_2O_3-80TeO_2$  ( $x = 2$  mol% to 20 mol%) glass samples.

#### 4. Discussion

The general increase in DC conductivity with  $Fe_2O_3$  content (Fig.2) in the glass system can be attributed to a decrease of the polaron hopping distance between the ions caused by  $Fe^{2+}/Fe^{3+}$  replacing  $Mn^{3+}/Mn^{4+}$  on a two to one ratio. Meanwhile, the saddle-like region between  $10 \text{ mol}\% \leq x \leq 15 \text{ mol}\%$  in our DC measurement is attributed to MTE, where the mixed  $Fe^{2+/3+}/Mn^{3+/4+}$  ions hinder polaronic transport. This behavior is suggested to be related to Anderson-like localization mechanism because of the random lattice potential in glasses. When Fe ion substitutes Mn ion in the glass system, at 10-15 mol% the different potentials of Mn and Fe appears to be randomized. In such a random potential, polaron hopping between the two different sites can be competitive and complex, causing localization. However, the DC conductivity did not reach a minimum at the MTE region as observed for the AC conductivity minimum in our previous work for the same glass system [38]. This can be understood that the total measured AC conductivity in the additive form characterized by the Jonhsher's universal power law,  $\sigma_{AC} = \sigma_{DC} + A\omega^s$  [48] implies that the AC and DC conductivities are independent and they arise from different mechanisms, while DC conductivity involves only single mechanism in the conductive response [49]. Moreover, the electrical properties of glasses in AC field depend not only on the mobile ions but also on the relatively immobile ions, which also take part in network forming [50]. As such, the localization effect for AC conductivity is naturally different from that of DC conductivity.

The saddle-like behavior in density ( $\rho$ ) between  $x = 10 \text{ mol}\%$  and  $x = 15 \text{ mol}\%$  is suggested to be influenced by the relatively smaller change in molar volume ( $V_a$ ) in the region that matches

the increase in mass as a result of the substitution. The reduction in the rate of  $V_a$  increase in the MTE region is intriguing because different contributions between two different ions may exist in the region. The result of the analysis of FTIR in our previous works for the same sample indicated that BO increased for  $x \leq 10$  mol%, whereas NBO increased for  $x > 10$  mol%. Due to the density anomaly, the discussion of this work will mainly focus on the  $10 \text{ mol}\% \leq x \leq 15 \text{ mol}\%$  region as it may reveal the physical nature of the MTE phenomena.

In the present work, the non-linear increase in  $V_a$  with  $\text{Fe}_2\text{O}_3$  content is attributed to elastic moduli behavior. The variation of  $C_L$ ,  $\mu$ ,  $K_e$ , and  $E$  with  $\text{Fe}_2\text{O}_3$  indicated that  $\text{Fe}_2\text{O}_3$  may occupy glass network positions and form strong covalent Fe–O bonds, which increased the rigidity of the glass. The replacement of  $\text{Fe}_2\text{O}_3$  in the glass system was expected to increase the formation of stronger glass networks, which increased elastic modulus because Fe–O possessed a stronger bond (409 kJ/mol) than Mn–O (402 kJ/mol). Although FTIR for the same glass system indicated the formation of bridging oxygens (BO) and non-bridging oxygens (NBO), these factors did not seem to contribute to the elastic behavior above. Our results did not indicate a monotonous increase in  $C_L$  and  $\mu$  and related elastic moduli with  $\text{Fe}_2\text{O}_3$  content as a sudden slight decline in elastic moduli at  $x = 15$  mol% occurred. Instead, our analysis of the results suggests that the elastic anomaly behavior may be related to MTE where conductivity minimum occurs in the same region ( $x = 15$  mol%) for the same glass system. This finding indicates that the MTE anomaly could cause elastic changes aside from affecting conductivity properties. Some elastic adjustments appeared to occur at  $x = 15$  mol% in terms of bond softening, which accompanied the reduction of  $V_a$  increase.

Poisson's ratio ( $\sigma$ ) describes the expansion of a sample in a direction perpendicular to the applied stress. Generally,  $\sigma$  is affected by a change in the crosslink density of a glass network. In the present study, Poisson's ratio ( $\sigma$ ) decreased from 0.26 to 0.25 for  $x \leq 10$  mol% accompanied by the increase in average crosslink density ( $\bar{n}_c$ ) from 2.1 to 2.4. However, for  $x > 10$  mol%, our results showed that the near constant region in  $\sigma$  is not followed by a near constant in the computed ideal cross link density ( $\bar{n}_c$ ). The near constant region observed for Poisson's ratio ( $\sigma$ ) for  $x > 10$  mol% (Fig. 6) indicated that the actual cross link density was unchanged in the region. In the context of electrical conductivity, the conductivity minimum region previously reported [38] was now determined to be unrelated to the changes in cross link. Also, the increase in  $C_L$ ,  $\mu$ , and related elastic moduli at  $x > 10$  mol% may not be associated with changes in cross link because  $\sigma$  was not altered significantly in the region. Thus, the increase in  $C_L$ ,  $\mu$ , and related elastic moduli relied on formation of stronger Fe–O bonds, which strengthen the rigidity of the glass structure during the initial addition of  $\text{Fe}_2\text{O}_3$  [51]. Meanwhile, hardness ( $H$ ) can be expressed as the resistance of a material to deformation, indentation, or penetration. In glasses, changes in  $H$  are usually related to the changes in crosslink density [41], interatomic bond strength [52], and free volume [1, 53]. However, the variation in  $H$  was not caused by the changes in crosslink density because  $\sigma$  does not significantly change in the present work. The roughly similar behavior of both  $H$  and  $E$  indicated that changes in hardness are strongly influenced by increasing the stiffness of the glass system.

Debye temperature  $\theta_D$  was associated with the highest allowable vibration mode, and this association reflected the overall structural stability and strength of bonds of solids [53]. Based on Eq. (6),  $\theta_D$  depends on the changes in the number of atoms in chemical composition ( $P$ ),  $V_a$ , and  $\nu_m$ . In general, however, the observation of the saddle-like behavior in the MTE region for  $\theta_D$  and  $\nu_m$  (Fig. 7) indicates that average rigidity and stiffness do not change within the narrow  $10 \text{ mol}\% \leq x \leq 15 \text{ mol}\%$  region. Overall,  $\theta_D$  increased with increasing  $\text{Fe}_2\text{O}_3$  content, thereby indicating that the overall rigidity of the glass system increased. Moreover, the observed saddle-like behavior of glass transition temperature ( $T_g$ ) for  $10 \text{ mol}\% \leq x \leq 15 \text{ mol}\%$  (Fig. 8) confirms that the average elastic moduli does not change in the region.

Our analysis of the experimental results using the bulk compression model [54], which demonstrated the higher calculated value of  $K_{bc}$  compared with that of  $K_e$ , indicates that the compression occurred through the mechanism that required less energy compared with that of the pure compression of the network bonds [47]. The decrease in  $K_{bc}/K_e$  with the addition of  $\text{Fe}_2\text{O}_3$  at

$x$  from 2 to 10 mol% (Fig. 9) indicated increased isotropic compression, whereas the increase at  $x = 15$  mol% demonstrated the increase in non-isotropic compression because of ring deformation orbending [55]. Meanwhile, the decrease in average ring size  $\ell$  (Fig. 9) also followed the  $K_{bc}/K_e$  behavior, thereby indicating the decrease of ring deformation. However, the main compression mechanism of the glass system was suggested to be mainly an isotropic compression because the  $K_{bc}/K_e$  values were between 1 and 3 [53]. Interestingly, the average ring size also reflected anomalies between 10 and 15 mol% ( $10 \text{ mol}\% \leq x \leq 15 \text{ mol}\%$ ), where the sudden increase in  $K_{bc}/K_e$  at  $x = 15$  mol% followed the abrupt increase of average ring size. The off-trend behavior in  $\ell$  and  $K_{bc}/K_e$  at  $x = 15$  mol% coincided with results of a previous report on conductivity minimum at the same position for the same glass system. The transition from  $\text{MnO}_2$ -to  $\text{Fe}_2\text{O}_3$ -based conductivity in the glass system appears to be accompanied by the abnormal increase in the average ring size at the point. This finding may explain the saddle-like behavior in the MTE region where the sudden increase in ring size affected the increase in  $\theta_D$  and  $v_m$  at  $x = 15$  mol%.

UV-Vis light absorption in oxide glasses is attributed to the excitation of electrons from the valence band associated with NBO [56]. The maximum  $E_{opt}$  when  $\text{Fe}_2\text{O}_3$  increased to  $x = 10$  mol% (Fig. 11) can be determined based on the changes in NBO [9, 56, 57]. Previous studies reported that NBO exhibits higher polarizability than BO and also binds excited electrons more loosely than BO. Thus, NBO requires lower energy to induce electron excitation than BO, resulting in a decrease in  $E_{opt}$  with increasing NBO [58, 59]. The decrease in  $E_{opt}$  for  $x > 10$  mol% (Fig. 11) may occur because of the increase in NBO, which possesses higher polarizability compared with that of the covalent bond of BO [60, 61]. On one hand, the behavior of  $n$  is shown in Fig. 11. The minimum of  $n$  at  $x = 10$  mol% supports our proposition that some form of blocking effect occurs on dipoles in the MTE region because a dielectric minimum was also previously reported at the same location. On the other hand, the large increase in  $n$  for  $x > 10$  mol% (Fig. 11) may be attributed to the increase in NBOs, which possess higher polarizability than BOs. This finding is consistent with our FTIR results for the same glass system in a previous report [38].

On the other hand, Dimitrov and Komatsu [44] calculated the values of optical basicity for single-component oxides. The high value of optical basicity of the present glass samples (Table 5) in the range of 1.204–1.241 [45] indicates lower covalency and higher basicity of the glass system. The replacement of  $\text{MnO}_2$  with lower optical basicity (0.95) [44] by  $\text{Fe}_2\text{O}_3$  with higher optical basicity (1.02) [44] is expected to increase glass basicity as observed for  $x > 10$  mol% where effective replacement of  $\text{Fe}_2\text{O}_3$  for  $\text{MnO}_2$  occurs. Meanwhile, the electronic polarizability (Table 5) exhibited high magnitude in the range of  $3.586\text{--}3.891 \text{ \AA}^3$  [61, 62] in the present work, which could be attributed to small cation unit field strengths (Table 3) of  $\text{Fe}^{3+}$  and  $\text{Mn}^{3+}$ . As a consequence, the refractive index also exhibited a high magnitude in the range of 3.120–3.381 for the present glass system. The similar variation of  $\alpha_0^2$  to  $A$  indicates that electronic polarizability changes are strongly influenced by the optical basicity of the glass system. The increase in electronic polarizability for  $x \geq 10$  mol% is directly proportional to refractive index and dielectric constant, which was consistent with the previous study of Dimitrov et al. [44]. This phenomenon occurred because of the increasing number of NBO with the concentration of  $\text{Fe}_2\text{O}_3$  where NBO has a high polarizing tendency compared with BO, as confirmed by FTIR results in our previous works [38].

#### 4. Conclusion

The DC conductivity and elastic nature of the MTE region of  $x\text{Fe}_2\text{O}_3\text{--}(20\text{--}x)\text{MnO}_2\text{--}80\text{TeO}_2$  glass was studied along with its optical properties. The saddle-like region between  $10 \text{ mol}\% \leq x \leq 15 \text{ mol}\%$  in DC conductivity was attributed to Anderson-like localization due to disorder of the glass system. Saddle-like regions also appear for longitudinal and shear velocities ( $v_L$  and  $v_S$ ), independent moduli ( $C_L$  and  $\mu$ ), and bulk modulus ( $K_e$ ) between  $10 \text{ mol}\% \leq x \leq 15 \text{ mol}\%$ . On the other hand, Debye temperature ( $\theta_D$ ) increased except for a saddle-like behavior between 10 mol% and 15 mol% ( $10 \text{ mol}\% \leq x \leq 15 \text{ mol}\%$ ), indicating that the overall rigidity and strength of the glass was relatively unchanged in the region. These anomalies were attributed to

the MTE where conductivity minimum was observed at  $x = 15$  mol%, as previously reported. Further analysis using bulk compression and ring deformation models indicated that the overall average ring size decreased from  $x = 2$  mol% to  $x = 20$  mol%, whereas  $K_{bc}/K_e$  ratio decreases except at  $x = 15$  mol% where a slight increase in average ring size and  $K_{bc}/K_e$  ratio was observed. However, the values of  $K_{bc}/K_e$ , which are between 2.08 and 2.45, indicate that the main compression mechanism of the glass system was isotropic ring compression. The observed optical energy gap,  $E_{opt}$  maximum, and refractive index minimum at  $x = 10$  mol% coincide with previously reported dielectric minimum at  $x = 10$  mol%, demonstrating that NBO is more polarizable on the properties. Electronic polarizability and optical basicity also reflect anomalies between 10 mol% and 15 mol% ( $10 \text{ mol}\% \leq x \leq 15 \text{ mol}\%$ ) where the sudden decrease in electronic polarizability and optical basicity at  $x = 10$  mol% follows the minimum of the refractive index.

### Acknowledgement

The project was financially supported by the Ministry of Education of Malaysia and Research Management Centre (RMC), Universiti Teknologi Mara through the FRGS grant [No. RMI 600-RMI/FRGS 5/3 (53/2014)]. The authors would like to express their gratitude to the Universiti Teknologi Mara and the Ministry of Education of Malaysia for the SLAI scholarship given to Rosdiyana Hisam.

### References

- [1] M.A. Sidkey, M.S. Gaafar. *Physica B*, **348**, 46 (2004).
- [2] R.Rolli, K.Gatterer, M.Watchler, M.Bettinelli, A. Speghinni, A. Ajo, D, *Spect.Act A*, **57(10)**, 2009 (2001).
- [3] M.A. Sidkey, R. El-Mallawany, R.I. Nakhla, A.A. El-Moneim, *J.Non-Cryst. Solids*, **215**, 75 (1997).
- [4] E.C. Cardillo, R.A. Montani, M.A. Frechero, *J.Non-Cryst. Solids*, **356**, 2760 (2010).
- [5] E.A. Mohamed, F. Ahmad, K.A. Aly, *J Non-Cryst. Solids*, **538**, 230 (2012).
- [6] C.N. Reddy, R.V. Anavekar, *Mater. Chem. Phys.*, **112**, 359 (2008).
- [7] Y.B. Saddeek, *Mater. Chem. Phys.*, **91**, 146(2005).
- [8] D. Souri, *J.Scientific Research*, **5**, 44 (2010).
- [9] D. Souri, *Measurement*, **44**, 1904 (2011).
- [10] M.A. Sidkey, A.A. El-Moneim, L.A. El-Latif, *Mater. Chem. Phys.*, **61**, 103 (1999).
- [11] R.El-Mallawany. *Mater. Chem. Phys.*, **53**, 93 (1998).
- [12] R. El-Mallawany, A.A. Abousehly, E.Yousef, *J. of Mater. Sci. Lett.*, **19**, 409 (2000).
- [13] N. V. Ovcharenko, T. V. Smirnova, *J. Non-Cryst Solids*, **291**, 121 (2001).
- [14] R. El-Mallawany, M.D. Abdalla, I. A Ahmed. *Mater. Chem. Phys.*, **29**, 109 (2008).
- [15] A.H. Khafagy, A.A. El-Adawy, A.A. Higazy, S.El-Rabaie, A.S. Eid, *J Non-Cryst. Solids*, **354**, 3152 (2008).
- [16] E.S. Yousef, B. Al-Qaisi, *Solid State Sci.*, **19**, 6 (2013).
- [17] G. Lakshiminarayana, H. Yang, J.Qiu, *J. Alloys Compd.*, **475**, 569 (2009).
- [18] E.Yousef, M.Hotzel, C.Russel, *J. Non-Cryst Solids*, **353**, 333 (2007).
- [19] F.F. Chen, B.A. Song, C.G. Lin, S.X. Dai, J.W. Cheng, J.Heo, *Mater. Chem. Phys.*, **135**, 73(2012).
- [20] T.F. Xu, F.F. Chen, S.X. Dai, X. Shen, X.S. Wang, Q.H. Nie, C. Liu, K. Xu, J. Heo, *J. Non-Cryst Solids*, **375**, 2219 (2011).
- [21] P.Nandi, G. Jose, *Opt. Commun.*, **265**, 588 (2006).
- [22] M.M.Ahmad, E.S.Yousef, E.S.Moustafa. *Phys. B*, **371**, 74 (2006).
- [23] V.Ravikumar, N.Veeraiah. *J. Phys. Chem. Solids*, **59**, 91 (1998).
- [24] T.Sankarappa, M.Prashant Kumar, G.B. Devidas, N.Nagaraja and R.Ramakrishnareddy. *J. Mol. Struct.*, **889**, 308 (2008).

- [25] Y.Gandhi, N.Krishna Mohan, N.Veeraiyah. *J. Non-Cryst Solids*,**357**, 1193 (2011).
- [26] J.C. Sabadel, P.Armand, D. Cachau-Herreillat, P.Baldeek, O.Doctot, A. Ibanez, E.Philippot, *J.Solid State Chem.*,**132**, 411 (1997).
- [27] V.Rajendran, N.Palanivelu, B.K.Chaudhuri, K.Goswami, *J. Non-Cryst Solids*,**320**, 195 (2003).
- [28] J.C. S.Moraes, J.A.Nardi, S. M.Sidel, B. G.Mantovani, K.Yukimitu, V.C.S.Reynoso, *J. Non-Cryst Solids*,**356**, 2146 (2010).
- [29] M.A.Sidkey, A.A.El-Moneim, L.A.El-Latif, *Mater. Chem. Phys.*,**61**, 103 (1999).
- [30] I.Ardelean, H.H.Qiu, H.Sakata, *J. Non-Cryst Solids*,**32**,335 (1997).
- [32] A.Ghosh, *J. Phys. Condens. Matter*,**1**, 7819 (1989).
- [33] M. M. El-Desoky, *J. Non-Cryst Solids*,**351**, 3139 (2005).
- [34] V.Rajendran, N.Palanivelu, B.K.Chaudhuri, K.Goswami, *J. Non-Cryst Solids*,**320**, 195 (2003).
- [35] Sezhian Annamalai, Rudra P. Bhatta, Ian L. Pegg, Biprodas Dutta, *J. Non-Cryst Solids*,**358**, 1380 (2012).
- [36] E.Mansour, Y.M.Moustafa, G.M.El-Damrawi, S.Abd El-Maksoud, H. Doweidar, *Phys. B*,**305**, 242 (2001).
- [37] Biprodas Dutta, Niveen A. Fahmy, Ian L. Pegg, *J. Non-Cryst Solids*,**351**, 1958 (2005).
- [38] Rosdiyana Hisam, Ahmad Kamal Yahya, Halimah Mohamed Kamari, Zainal Abidin Talib, Ri Hanum Yahaya Subban. *Mater. Express*, **6**, 149 (2016).
- [39] Dariush Sour, Seyed Ali Salehizadeh, *J. Therm Anal Calorim*,**112**, 689 (2013).
- [40] Darius Sour. *Measurement*,**44**, 1904 (2011).
- [41] S.Laila, A.K. Suraya, A.K. Yahya, *Chalcogenide Lett.*, **11**, 91(2014).
- [42] R. El-Mallawany. *Mater. Chem. Phys.*, **53**, 93 (1998).
- [43] R. El-Mallawany, N. El-Khoshkhany, H. Afifi, *Mater. Chem. Phys.*,**95**, 321 (2006).
- [44] V.Dimitrov and S.Sakka. *J.Appl. Phys.*,**79**, 1736 (1996).
- [45] V.Dimitrov and T.Komatsu. *Journal of The University of Chemical Technology and Metalurgy*,**45**, 219 (2010).
- [46] A.F. Wells. *Structure Inorganic Chemistry*, Clarendon Press, Oxford (1975).
- [47] R. El-Mallawany, N. El-Khoshkhany, H. Afifi, *Mater. Chem. Phys.*,**95**, 321 (2006).
- [48] A.K. Jonscher, *Nature (London)* **267**, 673 (1977).
- [49] A.K. Jonscher, *Dielectric Relaxation in Solids*, Chelsea Dielectric Press, London, (1983).
- [50] A.E. Owen, *Prog. Ceram. Sci*, **77** (1963).
- [51] S.Azianty, A.K Yahya, M.K. Halimah, *J. Non-Cryst Solids*,**358**,1562 (2012).
- [52] T.Watanabe, K.Muratsubaki, Y.Benino, H.Saitoh, T.Komatsu, *J. Mater. Sci*,**36**, 2427 (2001).
- [53] H.Afifi, S.Marzouk, *Mater. Chem.Phys.* **80**, 517 (2003).
- [54] B.Bridge, A.A. Higazy. *Phys. Chem. Glasses*,**27**, 1 (1986).
- [55] M.M. Umair, A.K. Yahya, *Mater. Chem. Phys.*,**142**, 549 (2013).
- [56] S.Rada, M.Rada, E.Culea, *J. Non-Cryst Solids*,**357**, 62 (2011).
- [57] G.Upender, V.C.Mouli, *J. Mol. Struct.*,**1006**, 159, (2011).
- [58] G.Upender, C.P. Vardhani, S.Suresh, A.M. Awasthi, V.C. Mouli, *Mater. Chem. Phys.*,**121**, 335 (2010).
- [59] P.G. Pavani, K.Sandhana, V.C. Mouli, *Phys.B*,**406**, 1242 (2011).
- [60] E.A. Mohamed, F.Ahmed, K.A.Aly, *J. Alloys Comp.*, **230**, 538 (2012).
- [61] S.F. Khor, Z.A. Talib, W.M.M. Yunus, *Ceram. Int.*, **38**, 935 (2012).
- [62] P.Limkitjaroenporn, J.Kaewkhao, W.Chewpraditkul. *J. Phys. Chem. Solids*,**72**, 245(2011).